Zinc Sulfide Nanosheet-Based Hybrid Superlattices with Tunable Architectures Showing Enhanced Photoelectrochemical Properties

*Peng-peng Wang, Hao-yi Li, Huiling Liu, Peilei He, Biao Xu, and Xun Wang**

Semiconductor nanocrystals (NCs) and their self-assembled superstructures have attracted extensive interests in terms of their extraordinary charms in quantum confinement effect, fascinating electric and optic properties, and promising applications in energy conversion and next-generation nanodevices.[1–7] While the remarkable success in the controlled synthesis of NCs with various shapes has been achieved in the past two decades, the progress in a rational assembly of them into uniform and ordered superlattices has been slow. For instance, previous studies showed that isotropic spherical semiconductor NCs can self-assemble into versatile superstructures such as superparticles, film, and closed packed arrays that show tailored properties in catalysis, plasmonics, high-density data storage, and energy conversion.[8–10] However, for anisotropic NCs that can exhibit shape-dependent properties and lead to self-assembled structures with collective properties, there are limited assembly examples due in part to their strong shape-specific interactions.[4,11] Theoretically, the properties of superstructures depend on their architectures and the shapes, spatial arrangement, and degree of order of building blocks. Colloidal superlattices assembled from semiconductor nanostructures, especially those with anisotropic shapes, could increase the power of modulating characteristics such as electronic transport and optical response. In particular, 1D superlattices hold considerable promise for tuning photoelectric, sensing functions and could be most desirable for studying the quantum transport, light–matter interaction, and other physical phenomena along the longitudinal and radial directions.[12–17] Among these 1D superlattices, nanosheet-based superstructures, especially those with unique architectures that have collective properties, are intriguing but still underdeveloped.[15] Here, we report the construction of ZnS nanosheet-based hybrid superlattices with rod and tube architectures (denoted as SRs and STs, respectively) and tunably periodic distance by utilizing alkyl amines as structure-directing agents, in which ZnS nanosheets with uniform sizes self-assemble into vertical 1D superlattices via face-to-face interactions. The resulting structures can be converted to other functional nanostructures maintaining the original dimensionalities by cation-exchange reaction and serve as supporting materials for controllable deposition of noble metal NCs. More impressively, the ZnS nanosheet-based hybrid superlattices showed enhanced photoelectrochemical properties that are probably attributed to the ultrathin feature of ZnS nanosheets and their superstructures (**Scheme 1**).

The ZnS-based hybrid superstructures were formed by spontaneous assembly of ultrathin nanosheets as they grew in a simple amine solution (octylamine), in which the long-chain amine acted both as a ligating solvent and as a structure-directing agent. A detailed explanation on the synthetic procedures is given in the Experimental Section. The N–H modes in the range of 1600–1460 cm^{-1} and the CH_2 and CH_3 stretching vibrations of 2850–3000 cm^{-1} in the Fourier transformation infrared (FT-IR) spectrum indicate that the products are capped with octylamine (Figure S1, Supporting Information).[18] **Figure 1** highlights the structure of ZnS hybrid SRs obtained by using thiourea as a sulfur source and octylamine as a solvent. The scanning electron microscope (SEM, Figure 1a) image reveals that the obtained samples have rod morphology with uniform diameters of about 120–150 nm and the lengths up to 2 μm. From Figure 1a, we also notice that the ends of the rods have near hexagonal shape, suggesting their nanosheet-based building units aftermentioned. A low-magnification transmission electron microscope (TEM) image shows large areas of uniform rods, agreeing well with the SEM observation. Energy-dispersive X-ray (EDX) analysis confirms that the elemental ratio between Zn and S is 1:1 (Figure S2, Supporting Information), while the thermogravimetric analysis (TG) presents the organic content of the SRs (Figure S2f, Supporting Information). It is interesting to note that these rods are actually superlattice structures composed of ZnS ultrathin nanosheets (capped by amines). Furthermore, these nanosheet-based superstructures occurred spontaneously during the growth of ZnS NCs. A close examination of an SR (Figure 1c) clearly shows that these ZnS nanosheets are piled face-to-face into a periodic array with uniform intervals, thus forming highly regular periodicity extending over the rod (consistent with the ends of the SRs in the SEM image). This is further confirmed by the high-angle annular dark field (HAADF) STEM image, which exhibits clearly ordered stripes (corresponding to the

Dr. P.-P. Wang, H.-Y. Li, H. Liu, P. He, B. Xu, Prof. X. Wang
Department of Chemistry
Tsinghua University
Beijing 100084, China
E-mail: wangxun@mail.tsinghua.edu.cn

DOI: 10.1002/smll.201500610

www.MaterialsViews.com

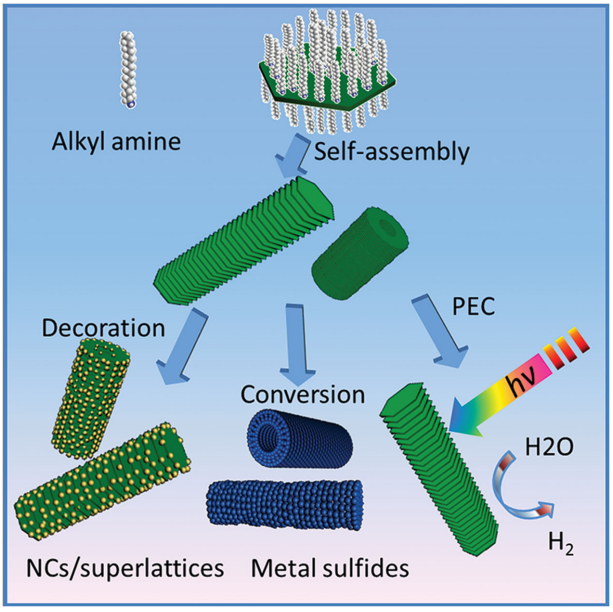

Scheme 1. Schematic representation of the formation of ZnS ultrathin nanosheet-based hybrid superlattices with rod-like and tubular morphologies. The resulting superstructures show excellent photoelectrochemical properties and enable versatile derived structures.

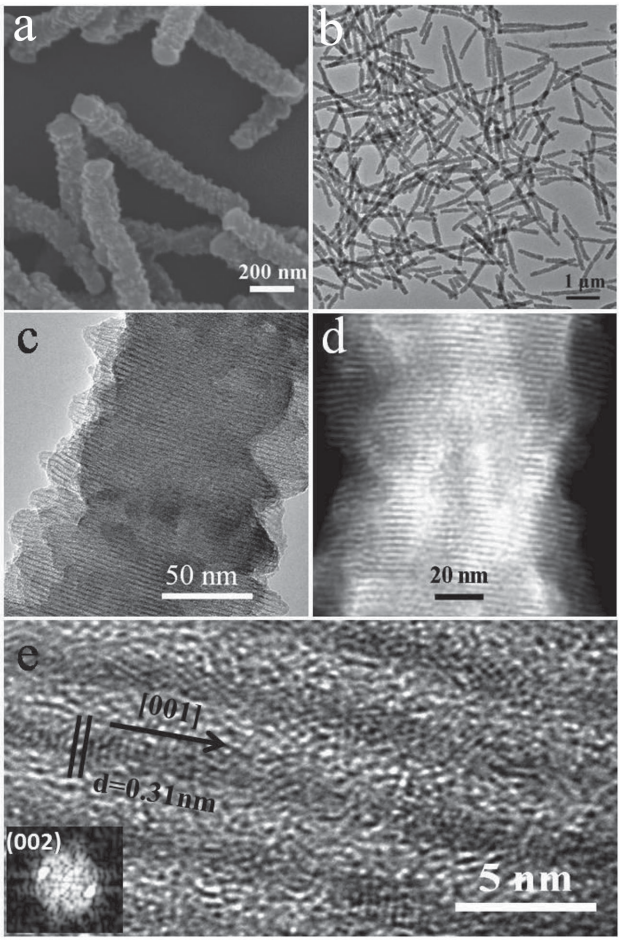

Figure 1. a) Typical SEM image, b,c) TEM images, d) STEM image, and e) HRTEM image of the as-obtained ZnS hybrid SRs. The inset in (e) is the fast Fourier transform pattern of one ZnS layer, showing clearly the crystalline nature.

side of ZnS nanosheets) along the longitudinal direction (Figure 1d). The high-resolution (HR) TEM image demonstrates the crystalline nature of ZnS layers with thickness of 1.5 nm and a interlayer distance of 2.8 nm in the superstructures (Figure 1e). The interplane distance is ≈0.31 nm, which corresponds to that of the (002) facet of ZnS. This indicates that the growth of the ZnS layers is along the [001] direction. The superstructures can even be kept well after 200 °C treatment in vacuum, suggesting their high thermal stability (Figures S3, S4, Supporting Information). The powder X-ray diffraction (XRD) pattern of the SRs is shown in **Figure 2**a, in which the Bragg peaks in the wide angle are consistent with the ZnS wurtzite phase but with a little shift. This shift is probably due to lattice strain caused by ultrathin NCs and their ligands, which could be usually observed in NCs in the literature.[19] In the small-angle regions, the pattern displays a group (00*l*) Bragg peaks typical of layered characters, suggesting that the superstructures could occur spontaneously during the synthesis. The most intense peak at $2\theta = 3.2°$ suggests an interlayer distance of 2.76 nm, which is consistent with the TEM observation.

Tunable periodicity is vital for engineering couplings in the semiconductor superlattice system. In our case, we can achieve continuously tunable periodicity by choosing amines with different chain length as structure-directing agents. For instance, substitution of C12 amine for octylamine in the synthetic reaction would also lead to uniform SRs (Figure S5, Supporting Information) but with a larger interlayer distance of 3.74 nm. Meanwhile, the SRs obtained in octylamine can undergo ligand exchange with oleylamine that further increases the interspacing of superlattices to 5.32 nm (Figure S6, Supporting Information). As shown in Figure 2b, the (001) and higher order peaks of the superlattices are gradually shifted to lower 2θ angles as the chain length of amine increases, confirming the gradual increase of superlattice periodicity.

Short-chain amines are usually used as organic restricting agents in the synthesis of inorganic–organic hybrid semiconductor materials. Similarly, we found that long-chain amines played a key role in the formation of superlattices, which is indirectly evidenced by the tunable periodicities ranging from 2.8 to 5.3 nm with different amines as structure-directing agents. This structure-directing effect of amines can also be found in many literatures, in which amine molecules acted as linkers to bridge semiconductor atomic layers, forming periodic 3D lattices.[20,21] In our case, the ZnS superlattices are directed by the long-chain amines that are usually used in the synthesis and self-assembly of NCs.[22,23] As a result, the obtained structures appeared as "layer-by-layer" assembly of ultrathin nanosheets separated by the long-chain amines, ensuring the largest contact area between NCs. Similar phenomena have been observed in the self-assembly of other ultrathin NCs.[22] Our previous study has shown that alcohols usually act as poor solvents in the amine-based reaction system and consequently affect the interactions among primary building blocks and final assembly structures.[18] In the

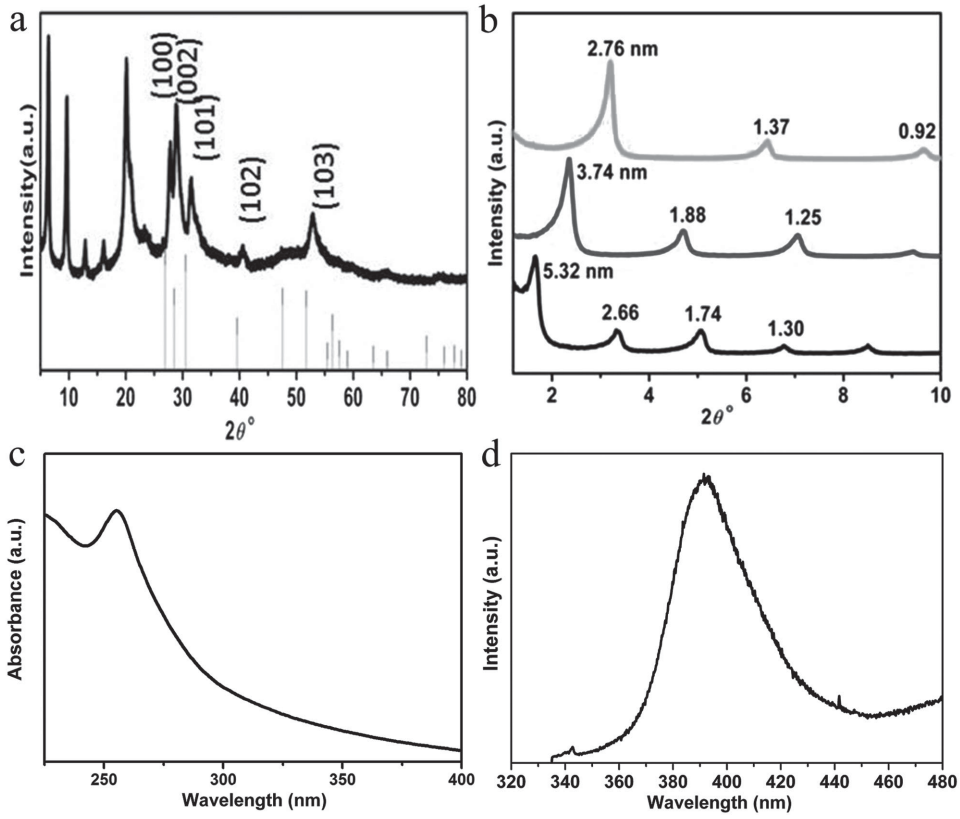

Figure 2. a) XRD pattern of the ZnS hybrid SRs synthesized in octylamine (the black lines below correspond to pure ZnS phase derived from JCPDS card). b) Small-angle XRD of the SRs capped with octylamine (upper), dodecylamine (middle), and oleylamine (lower), indicating that the interlayer distances are 2.76, 3.74, and 5.32 nm, respectively. c) UV–vis absorption spectrum and d) PL spectrum of the SRs.

current case, when adding ethanol in the system and reacting at a higher temperature, the as-obtained samples showed nanosheet structures without assembly behaviors, which further confirms the superstructures formed in the amine system (Figure S7, Supporting Information). Owing to the ultrathin building blocks (ZnS ultrathin nanosheets) here, the entire XRD pattern (Figure 2a) is similar to that of ZnS (hexamine) hybrid materials reported but with larger interlayer distance and crystalline inorganic layers with thickness of 1.5 nm.[24]

Considering the uniform size of ultrathin NCs in the superstructures, we carried out UV–vis absorption and photoluminescence (PL) characterizations to study their optical properties. Figure 2c shows a representative UV–vis spectrum of SRs obtained in octylamine, in which a sharp absorption peak at 255 nm can be observed. Compared with the bandgap of bulk ZnS, it is clear that there is a large blue shift, which is due to a quantum confinement effect as the result of ultrathin nanostructures.[25] Such a strong and sharp absorption peak indicates the uniformity of crystalline ZnS nanolayers in our hybrid SRs. Meanwhile, we observed no significant differences between the UV–vis spectra of SRs with different periodic distances (Figure S8, Supporting Information), which implies that the similar ZnS sizes are obtained for all hybrid superlattices despite different periodicities. The room temperature PL spectrum is shown in Figure 2d. For ZnS NCs, the emissions usually come from direct band-to-band recombination, shallowly trapped recombination via lattice vacancies and deep-trap emission attributed to surface defect sites.[26] Here, a peak with a maximum at around 390 nm was observed, which could be attributed to the intrinsic emission of ZnS. Since the observed emission band from the confined ZnS layers in the superlattices has a spectral range of 350–450 nm, it is also possible that vacancies emission or interstitial zinc emission can be a contributor.[26,27] No obvious PL difference was observed for superlattices with different periodicities, again confirming the similar size of inorganic components in all superstructures.

It is well known that different sulfur sources are widely used to synthesize shape-controlled sulfide NCs although the mechanism of precursor reaction remains to be developed.[28–30] In our case, substitution of sulfur for thiourea as an alternative sulfur source in the reaction leads to the formation of STs, which is possibly due to different reaction pathways and kinetics compared with those for the thiourea-involved reaction. **Figure 3** and Figure S9a (Supporting Information) show the morphologies of STs with diameters of 190–240 nm and lengths up to 2 μm. High-magnification TEM images reveal the superlattice structures, where the ZnS nanolayers packed orderly along the longitudinal direction (Figure 3a–c). The cavity is visible in a 1D structure in the HAADF STEM (Figure 3d) and EDS mapping images (the insets in Figure 3b), thus reinforcing the TEM observation of tubes (the inset in Figure 3a exhibits clearly the cavity and the nanosheet building blocks). The XRD, EDX, and TG analyses (Figure S9c,d, Supporting Information) show similar results compared with SRs. HRTEM images (Figure 3e,f)

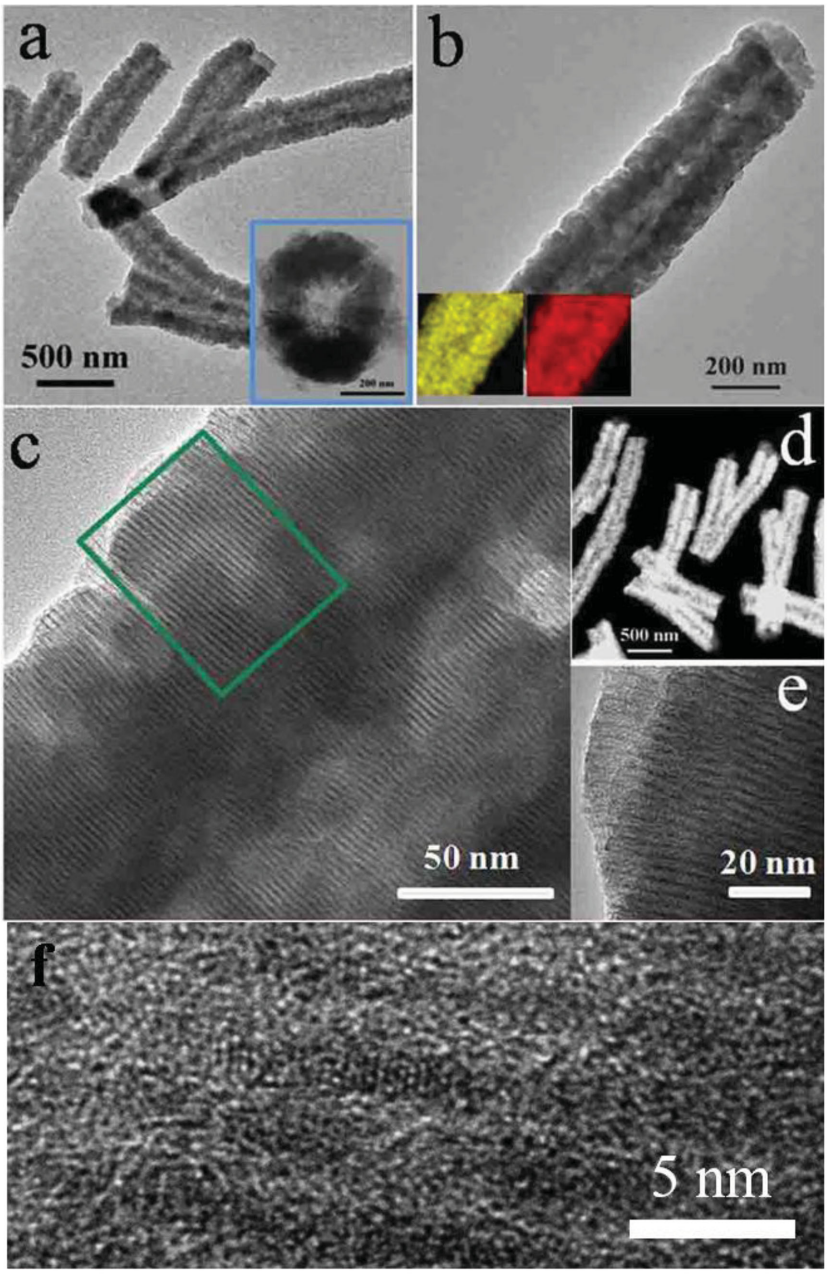

Figure 3. a–c) TEM images and d) STEM image of the as-obtained ZnS hybrid STs. The inset in (a) is a sectional view of a short tube, showing clearly the cavity and nanosheet structures. The insets in (b) are EDX elemental maps, which clearly indicate that zinc and sulfur are uniformly distributed in the STs (the superstructures are not seen because of limited resolution). e,f) HRTEM images of the SRs.

show the stripe pattern where the dark-contrast regions are ZnS nanolayers with similar thickness compared with the SRs.

These ZnS (amine) hybrid 1D structures can serve as starting nanostructures for the facile preparation of other 1D functional nanomaterials. Recently, much attention has been paid to cation-exchange reaction owing to its convenience in the preparation of NCs.[31,32] Here, we adopt this strategy to fabricate 1D CuS nanostructures under mild conditions, as a proof of concept (the details in the Experimental Section). When the SRs reacted with excess Cu^{2+} cations in ethanol, CuS nanorods with similar size formed immediately (see **Figure 4**a,b). However, the layered structures were destroyed. The HRTEM image (Figure 4c) shows lattice fringes with different orientations, suggesting that the rods are composed of CuS NCs. The composition is further confirmed by EDS (Figure S10, Supporting Information) and XRD characterizations (Figure 4d). Note that some voids can be found on the CuS rods, which is attributed to the dissolution of octylamine ligands in the solution.[32] Similarly, when ZnS STs are used as starting materials, nanotubes composed of CuS NCs can be obtained (Figure 4e,f, and Figure S11, Supporting Information).

In addition to transformation to other 1D function nanostructures, the superstructures can also be used for preparing metal–semiconductor nanocomposites, which may enable advances in wide areas such as photochemistry and catalysis.[33,34] For example, gold NCs can be deposited onto ZnS-based SRs by using $HAuCl_4$ as a gold precursor and octylamine as a stabilizing agent for the NCs and a reduction agent. Figure S12 (Supporting Information) presents a TEM image of Au NCs on the SRs, in which the NCs, identified by the dark contrast owing to its high electron density, homogeneously deposit throughout the SRs, and their average size is ≈2 nm. It is well known that the redox reactions between gold salt and sulfides can occur in NC systems.[35,36] In our case, without an additional reducing agent, Au nanoparticles can also grow on the SRs due to the above-mentioned redox reaction and the presence of octylamine ligands in the SRs. When gold salt is mixed with ethanol dispersion of ZnS hybrid SRs, the white dispersion gradually changed to brown, implying the formation of ultrafine gold NCs. As the gold concentration is increased a marked color change is observed (Figure S13, Supporting Information), implying that more and more gold nanoparticles grew on the SRs. These metal–semiconductor nanocomposites may provide opportunities for further tuning of the functionality of the as-prepared superstructures.

In general, photoelectrochemical cells (PECs) offer a promising tool for evaluating energy conversion of a semiconductor material. Here, photocurrent response is tested for comparative studies on the catalytic activity of the superlattices with different periodicities, nanosheets, and commercial ZnS. Under ultraviolet radiation, the photocurrent response of the samples, ZnS nanosheet-based

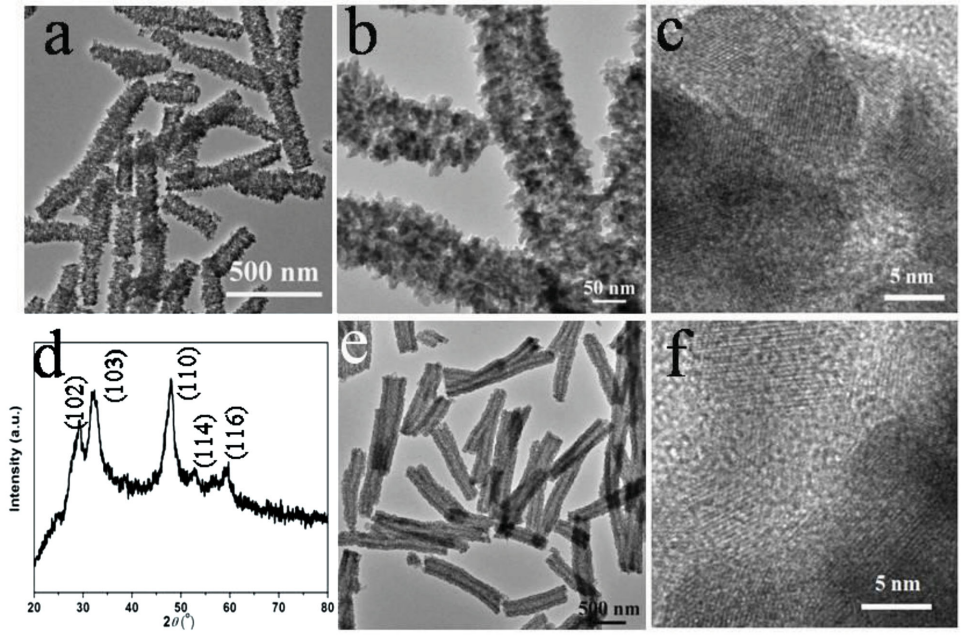

Figure 4. a,b) TEM image and c) HRTEM image of CuS nanorods obtained by cation exchange with ZnS SRs. d) XRD pattern of CuS nanorod (JCPDS card, 02-0820), e) TEM image, and f) HRTEM image of nanotubes composed of CuS NCs.

superlattices, which show white color, will be generated constantly as the potential becomes more and more negative. As shown in **Figure 5**a, the photocurrent density differences between light on and off increase with increasingly negative potential for both of the SRs (octylamine) and the SRs (dodecylamine). At $\eta = -1.2$ V (vs SCE), the photocurrent density response of the SRs (octylamine) can reach about 0.7 mA cm^{-2}, which is higher than those of the SRs (dodecylamines) (0.5 mA cm^{-2}) and the SRs (oleylamine) (the photocurrent density response is 0.34 mA cm^{-2}, Figure S14a, Supporting Information). Moreover, the sample shows quite steady performance of stability for the photocurrent response (Figure 5b). Besides, the impedances of the samples after thermal treatment have great reduction than those before thermal treatment, proving the promotion of electrical conductivity (Figure S15, Supporting Information). Compared with nanosheets (the red curve in Figure 5a) and commercial ZnS (Figure S16, Supporting Information), the superstructures here show much higher photoelectrochemical properties. On the one hand, the superlattices have comparable or even smaller surface areas compared with nanosheets that, in the real applications, usually restack resulting in the reduction of the effective active sites. On the other hand, the superlattices have larger surface areas compared with commercial ZnS powders. Hence, the enhanced performance of the superstructures may originate from large active surface area of nanosheet building blocks and the superstructures that can effectively avoid the agglomeration of catalysts, as well as the shortest interlayer space (SRs (octylamine)) in the as-prepared samples that facilitated the charge transport by considering that the photocurrent changing trend is increasing with a gradual decrease of interlayer space. Compared with the SRs, the STs show poor performance probably caused by the hollow structure in the center, which advises to the electron transport (Figure S14b, Supporting Information). In a word, the ZnS nanosheet-based hybrid superstructures presented here show promising and inspiring performance in PECs. Systematic studies are needed to further explore their performance.

In summary, we have successfully achieved ZnS ultrathin nanosheet-based hybrid superlattices with 1D rod and tube architectures. The periodicity of the superlattices can be easily tuned by varying the chain length of alkyl amines. The obtained superstructures showed excellent photoelectrochemical properties, owing to the unique ultrathin feature and superstructure that can effectively prevent the decrease of active surface area. Moreover, they can serve as starting materials for conversion to other functional nanomaterials with unchanged dimensionality and supporting materials for controllable decoration of ultrafine noble metal NCs, showing great potential in facile functionalization. We believe that, additionally, these 1D superstructures, which display sharp line width absorption and well-arranged periodicity extending over the entire 1D structures, would be ideal building blocks for further assembling into nanodevices with tailored properties and also provide an ideal platform for studying fundamental physical phenomena such as electro-optical modulating or exciton–light interactions on the nanoscale.

Experimental Section

Synthesis of ZnS Ultrathin Nanosheet-Based Hybrid Superlattice Rods: In a typical synthesis, 0.22 g of zinc acetate ($Zn(Ac)_2{\cdot}2H_2O$) and 0.15 g of thiourea (CH_4N_2S) were dissolved in 20 mL of octylamine (or dodecylamine) in a 40 mL Teflon-lined autoclave. Then, the solution system was heated at 60 °C for

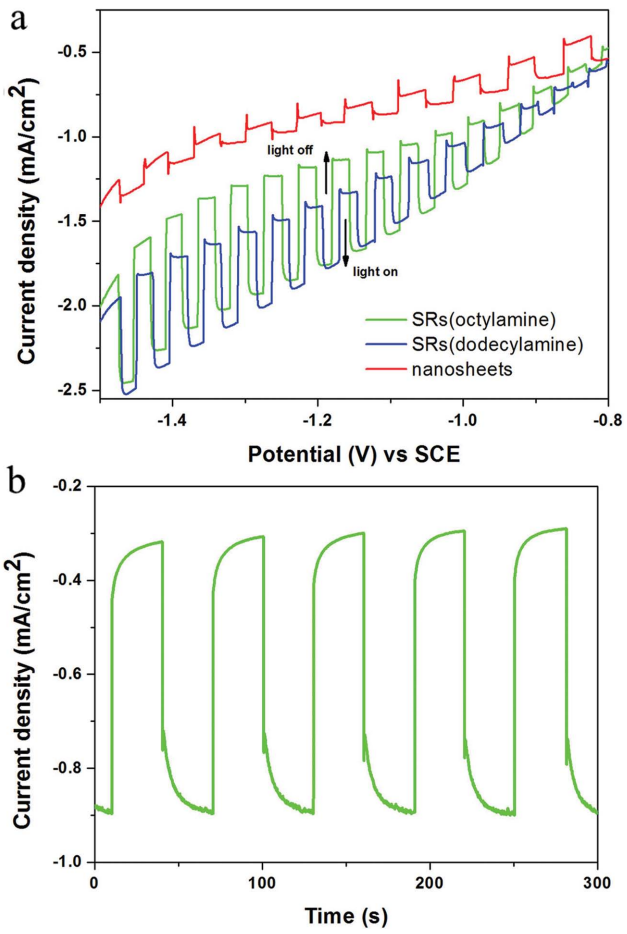

Figure 5. a) Photocurrent response for 200 °C heat-treated SRs (octylamine) (the green curve), SRs (dodecylamine) (the blue curve), and nanosheets (the red curve) at 10 mV s^{-1} in the 0.05 m Na_2S/Na_2SO_3 hybrid solution under 300 W Xe lamp ultraviolet radiation. The illumination on and off periods are 5 s. b) Photocurrent response stability for 200 °C heat-treated SRs (octylamine) under pulsed illumination (30 s ON/OFF) at a constant potential of –1.2 V (vs SCE).

12 h in an oven, and then cooled down to room temperature. The product was collected by centrifugation and washed several times with ethanol. The final white products were then dried in a vacuum at 50 °C overnight.

Synthesis of ZnS-Based Superlattice Tubes: 0.18 g of zinc acetate and 0.10 g of S powder were dissolved in 20 mL of octylamine. The whole system was ultrasonicated and stirred for getting a homogeneous solution, and then heated at 60 °C for 12 h. After the reaction was complete, the product was collected by adding ethanol and centrifugation.

Preparation of Au NPs Decorating ZnS-Based Superlattices: 2 mg of as-synthesized ZnS SRs was dispersed in 15 mL of octylamine, to which a certain amount of $HAuCl_4$ solution was added and stirred for 1 h at room temperature. The resulting products were separated by centrifugation and washed with ethanol.

Preparation of Au/ZnS Hybrid Superlattices in Ethanol: 2 mg of as-synthesized ZnS SRs was dispersed in 15 mL of ethanol, to which different amounts of $HAuCl_4$ solution ($HAuCl_4 \cdot 4H_2O$ in ethanol, 6.07 mmol L^{-1}) were added and stirred for 1 h at room temperature.

Preparation of CuS Nanorods and Nanotubes: 10 mg of as-synthesized ZnS SRs or STs was dispersed in 15 mL of ethanol, to which 15 mL of copper acetate solution (in ethanol) was added with stirring. The white ZnS solution quickly changed to brown, indicating the formation of CuS NCs. After 20 min, the precipitates were separated and washed with ethanol.

Characterization: XRD characterization was carried on a Bruker D8 Advance X-ray diffractometer using Cu Kα radiation (λ = 1.5418 Å). The morphologies and structures of the products were observed by using a Hitachi H-7700 TEM operating at 100 kV. Detail structure information was given by a Tecnai G2 F20 S-Twin high-resolution transmission electron microscope at 200 kV (HRTEM) equipped with high angle annular dark-field scanning TEM (HAADF-STEM). Fourier transform infrared spectra (FT-IR) were recorded with a Nicolet 205 FTIR spectrometer using the KBr pellet technique. UV–vis absorption spectra were measured on a Hitachi U-3010 spectrophotometer. Fluorescence spectra were recorded using a Horiba Jobin Yvon LabRAM HR800 Raman spectrometer.

Photoelectrochemical Measurements: Photoelectronchemical cells (PECs) measurement was carried out on a CHI 650D electrochemical workstation. The working electrode was prepared by drop casting the superstructures (after thermal treatment at 200 °C in vacuum) dispersion (100 µL × 2, with the concentration of 2 mg mL^{-1} in ethanol) onto F-doped tin oxide glass substrates. Photocurrent response measurements were taken in a typical three-electrode electrochemical system using a Pt gauze counter and saturated calomel electrode as the reference. PECs measurement involved the *I–V* scan and *I–T* scan technique using a 300 W Xe lamp. Potentiostatic alternating current impedance measurements were carried out in the same configuration at $\eta = -1$ V (vs SCE) from 10^5 to 0.1 Hz. The electrolyte was an aqueous Na_2S/Na_2SO_3 solution (0.05 m). During the test, N_2 was bubbled into the solution and the temperature was kept at 25 °C.

Supporting Information

Supporting Information is available from the Wiley Online Library or from the author.

Acknowledgements

P.-P.W. and H.-Y.L. contributed equally to this work. This work was supported by NSFC (21431003, 91127040, 21221062), and the State Key Project of Fundamental Research for Nanoscience and Nanotechnology (2011CB932402).

[1] M. Bruchez, M. Moronne, P. Gin, S. Weiss, A. P. Alivisatos, *Science* **1998**, *281*, 2013.
[2] J. H. Warner, R. D. Tilley, *Adv. Mater.* **2005**, *17*, 2997.
[3] C. B. Murray, C. R. Kagan, M. G. Bawendi, *Science* **1995**, *270*, 1335.
[4] T. Wang, J. Zhuang, J. Lynch, O. Chen, Z. Wang, X. Wang, D. LaMontagne, H. Wu, Z. Wang, Y. C. Cao, *Science* **2012**, *338*, 358.

[5] D. H. Webber, R. L. Brutchey, *J. Am. Chem. Soc.* **2012**, *134*, 1085.
[6] J. Embden, K. Latham, N. W. Duffy, Y. Tachibana, *J. Am. Chem. Soc.* **2013**, *135*, 11562.
[7] B. Xu, P. He, H. Liu, P. Wang, G. Zhou, X. Wang, *Angew. Chem. Int. Ed.* **2014**, *53*, 2339.
[8] P. Simon, L. Bahrig, I. A. Baburin, P. Formanek, F. Roder, J. Sickmann, S. G. Hickey, A. Echmuller, H. Lichte, R. Kniep, E. Rosseeva, *Adv. Mater.* **2014**, *26*, 3042.
[9] Z. Tang, Z. Zhang, Y. Wang, S. C. Glotzer, N. A. Kotov, *Science* **2006**, *314*, 274.
[10] T. Huang, Q. Zhao, J. Xiao, L. Qi, *ACS Nano* **2010**, *4*, 4707.
[11] T. Paik, C. B. Murray, *Nano Lett.* **2013**, *13*, 2952.
[12] F. H. Xue, G. T. Fei, B. Wu, P. Cui, L. D. Zhang, *J. Am. Chem. Soc.* **2005**, *127*, 15348.
[13] S. D. Carnevale, J. Yang, P. J. Phillips, M. J. Mills, R. C. Myers, *Nano Lett.* **2011**, *11*, 866.
[14] M. S. Gudiksen, L. J. Lauhon, J. Wang, D. C. Smith, C. M. Lieber, *Nature* **2002**, *415*, 617.
[15] C. Y. Hu, K. Q. Lin, X. L. Wang, S. J. Liu, J. Yi, Y. Tian, B. H. Wu, G. X. Chen, H. Y. Yang, Y. Dai, H. Li, N. F. Zheng, *J. Am. Chem. Soc.* **2014**, *136*, 12856.
[16] J. Zhang, Y. Tang, K. Lee, M. Ouyang, *Nature* **2010**, *466*, 91.
[17] C. M. Lieber, *Nano Lett.* **2002**, *2*, 81.
[18] P.-P. Wang, H. Y. Sun, Y. J. Ji, W. H. Li, X. Wang, *Adv. Mater.* **2014**, *26*, 964.
[19] Y. Du, Z. Yin, J. Zhu, X. Huang, X.-J. Wu, Z. Zeng, Q. Yan, H. Zhang, *Nat. Commun.* **2012**, *3*, 1177.
[20] Y. H. Liu, S. H. Porter, J. E. Goldberger, *J. Am. Chem. Soc.* **2012**, *134*, 5044.
[21] M. R. Gao, W. T. Yao, H. B. Yao, S. H. Yu, *J. Am. Chem. Soc* **2009**, *131*, 7486.
[22] Z. Y. Huo, C. K. Tsung, W. Y. Huang, M. Fardy, R. X. Yan, X. F. Zhang, Y. D. Li, P. D. Yang, *Nano Lett.* **2009**, *9*, 1260.
[23] Y. C. Cao, *J. Am. Chem. Soc.* **2004**, *126*, 7456.
[24] X. Y. Huang, J. Li, *J. Am. Chem. Soc.* **2007**, *129*, 3157.
[25] A. B. Panda, G. Glaspell, M. S. El-Shall, *J. Am. Chem. Soc.* **2006**, *128*, 2790.
[26] W.-S. Chae, J.-H. Yoon, H. Yu, D.-J. Jang, Y.-R. Kim, *J. Phys. Chem. B* **2004**, *108*, 11509.
[27] J. H. Yu, J. Joo, H. M. Park, S.-I. Baik, Y. W. Kim, S. C. Kim, T. Hyeon, *J. Am. Chem. Soc.* **2005**, *127*, 5662.
[28] J. W. Thomson, K. Nagashima, P. M. Macdonald, G. A. Ozin, *J. Am. Chem. Soc.* **2011**, *133*, 5036.
[29] M. Kruszynska, H. Borchert, J. Parisi, J. Kolny-Olesiak, *J. Nanopart. Res.* **2011**, *13*, 5815.
[30] X. Liang, P. Guo, G. Wang, R. Deng, D. Pan, X. Wei, *RSC Adv.* **2012**, *2*, 5044.
[31] D. H. Son, S. M. Hughes, Y. Yin, A. Paul Alivisatos, *Science* **2004**, *306*, 1009.
[32] Y. Yu, J. Zhang, X. Wu, W. Zhao, B. Zhang, *Angew. Chem. Int. Ed.* **2012**, *51*, 897.
[33] Y. Feng, I. S. Cho, P. M. Rao, L. Cai, X. Zheng, *Nano Lett.* **2013**, *13*, 855.
[34] T. Mokari, C. G. Sztrum, A. Salant, E. Rabani, U. Banin, *Nat. Mater.* **2005**, *4*, 855.
[35] L. Carbone, S. Kudera, C. Giannini, G. Ciccarella, R. Cingolani, P. D. Cozzoli, L. Manna, *J. Mater. Chem.* **2006**, *16*, 3952.
[36] J. Yang, J. Peng, Q. Zhang, F. Peng, H. Wang, H. Yu, *Angew. Chem. Int. Ed.* **2009**, *48*, 3991.

Received: March 3, 2015
Revised: March 29, 2015
Published online: May 4, 2015